SCREENING AND EVALUATION OF PERFORMANCE INDEXES FOR MULTICOMPONENT GAS ABSORPTION SPECTRA OF COAL SPONTANEOUS COMBUSTION**

W. Wang [1,2], H. Liu [1,2], B. Yang [1,2], T. Ma [1,2], J. Li [1,2], J. Deng [1,2], D. Zhang [1,2]*

[1] School of Safety Science and Engineering at Xi'an University of Science and Technology, Xi'an Shaanxi, China; e-mail: zhangd@xust.edu.cn
[2] Key Laboratory of Mine and Disaster Prevention and Control of Ministry of Education at Xi'an University of Science and Technology, Xi'an Shaanxi, China

Coal spontaneous combustion (CSC) has been a global hazard for decades, causing significant losses. Hydrocarbon gases, including carbon monoxide (CO), carbon dioxide (CO_2), methane (CH_4), ethylene (C_2H_4), acetylene (C_2H_2), and oxygen (O_2), have proved to be good inhibitors for forecasting CSC. However, the cross-interference and absorption spectrum overlaps prevent their practical applications. This study simulates the refined distribution of the absorption lines of these index gases in the infrared spectral range to solve these problems. By selecting the optimal absorption lines for each gas, their detection performance was experimentally tested, and the results were analyzed using the Allan variance method. The results reveal that the optimal absorption lines are centered at 1566.64, 1572.32, 1653.72, 1626.34, 1530.37, and 760.65 nm for CO, CO_2, CH_4, C_2H_4, C_2H_2, and O_2, respectively. Relative detection errors are 0.62, 0.51, 3.06, 4.20, 0.58, and 1.96%, and the detection limits are 3.47×10^{-6}, 4.56×10^{-6}, 0.53×10^{-6}, 2.85×10^{-6}, 0.33×10^{-6}, and 1581×10^{-6}, respectively. The detection sensitivity and comprehensive detection accuracy were significantly improved. This study will provide a basis for solving the problem of the cross-aliasing interference between index gases for bituminous CSC.

Keywords: *coal spontaneous combustion, multicomponent, index gases, trace detection, tunable semiconductor laser absorption spectroscopy.*

СКРИНИНГ И ОЦЕНКА ПОКАЗАТЕЛЕЙ ЭФФЕКТИВНОСТИ СПЕКТРОВ ПОГЛОЩЕНИЯ МНОГОКОМПОНЕНТНЫХ ГАЗОВ ПРИ САМОВОЗГОРАНИИ УГЛЕЙ

W. Wang [1,2], H. Liu [1,2], B. Yang [1,2], T. Ma [1,2], J. Li [1,2], J. Deng [1,2], D. Zhang [1,2]*

УДК 535.34:543.27

[1] Школа науки и техники безопасности Сианьского университета науки и техники, Сиань Шэньси, Китай; e-mail: zhangd@xust.edu.cn
[2] Главная лаборатория по борьбе со стихийными бедствиями Министерства образования Сианьского университета науки и техники, Сиань, Шэньси, Китай

(Поступила 10 января 2022)

Для решения проблем перекрестной интерференции и перекрытия спектров поглощения индексных углеводородных газов, в том числе монооксида углерода (CO), двуокиси углерода (CO_2), метана (CH_4), этилена (C_2H_4), ацетилена (C_2H_2) и кислорода (O_2), при самовозгорании угля моделируется уточненное распределение их линий поглощения в ИК-диапазоне спектра. Путем выбора оптимальных линий поглощения для каждого газа экспериментально проверена их эффективность обнаружения, результаты проанализированы с использованием дисперсионного метода Аллана. Оптимальные линии поглощения CO, CO_2, CH_4, C_2H_4, C_2H_2 и O_2 расположены при 1566.64, 1572.32, 1653.72, 1626.34, 1530.37 и 760.65 нм соответственно. Относительные ошибки обнаружения 0.62, 0.51, 3.06, 4.20, 0.58 и 1.96%, пределы обнаружения 3.47×10^{-6}, 4.56×10^{-6}, 0.53×10^{-6}, 2.85×10^{-6}, 0.33×10^{-6}

**Full text is published in JAS V. 90, No. 1 (http://springer.com/journal/10812) and in electronic version of ZhPS V. 90, No. 1 (http://www.elibrary.ru/title_about.asp?id=7318; sales@elibrary.ru).

и 1581×10^{-6} соответственно. Значительно улучшены чувствительность и точность обнаружения. Полученные результаты обеспечивают основу для решения проблемы перекрестной интерференции между индексными газами при контроле самовозгорания при добыче битуминозных углей.

Ключевые слова: *самовозгорание угля, многокомпонентность, индексные газы, обнаружение следов, перестраиваемая полупроводниковая лазерная абсорбционная спектроскопия.*

Introduction. Coal spontaneous combustion (CSC) disasters occur worldwide, causing significant loss of coal resources and environmental pollution yearly [1–3]. CSC fires differ from other solid fires because they exhibit spontaneous combustion, smoldering, and re-ignition characteristics. They are extremely difficult to prevent and control owing to their hidden fire sources and easy to re-ignite [4, 5]. The determination of the degree of CSC danger has been a worldwide problem [6, 7], and many scholars have conducted extensive research from various perspectives.

Owing to the poor thermal conductivity of coal, gas detection is generally used to determine the risk of CSC [8, 9]. According to the detection principle, gas detection methods can be divided into non-optical and optical. Non-optical methods mainly include semiconductor gas sensing [10], electrochemical [11], paramagnetic [12], gas chromatography [13], and ultrasonic analysis methods [14]. However, the application of these methods is restricted owing to long response times and poor timeliness, as well as being greatly affected by temperature, pressure, vibration, and dust particles. Some of these methods can only be used for limited gas types, and the maintenance costs are high. These shortcomings of the above methods have led to the rapid development of fast and accurate dynamic detection methods, such as optical detection methods. Optical methods mainly include nondispersive infrared (NDIR) analysis [15], ultraviolet (UV) analysis [16], chemiluminescence (CL) [17], optical interference (OI) [18], Fourier transform infrared spectroscopy (FTIR) [19], differential absorption lidar (DIAL) [20], differential absorption spectroscopy (DOAS) [21], laser-induced fluorescence (LIF) [22], Raman laser spectroscopy (RLGA) [23], photoacoustic spectroscopy (PAS) [24], and tunable semiconductor laser absorption spectroscopy (TDLAS) methods [25]. These optical methods have the following disadvantages: NDIR is susceptible to cross-interference from adjacent wavelength gas spectrum lines; the cost of UV is high; CL requires manual detection and has high costs; OI cannot measure multiple component gases at the same time; FTIR calculation is time-consuming and easily affected by the environment; DIAL technology is very complicated; DOAS detection process has many impacting factors; LIF is only suitable for limited gas types; RLGA cannot be used in detecting trace gases; PAS has a poor signal resolution. Thus, new detection technologies for forecasting CSC are urgently needed.

TDLAS is a newly developed technology for real-time gas detection with high sensitivity and narrow spectral resolutions. This technology is suitable for accurately measuring trace gases [26]. To date, various TDLAS systems have been developed for gaseous analytes with sub-ppm concentrations. Werle et al. [27] used a vertical external-cavity surface-emitting laser to detect O_2 concentration at 760 nm. Gustafsson et al. [28] simultaneously monitored CH_4, O_2, and H_2O and detected indoor methane gas with a concentration of 3 ppm. Murzyn et al. [29] used TDLAS technology and proposed a new method for the quantitative measurement of temperature, pressure, and water vapor concentration during explosions. Guo et al. developed a portable laser sensor for trace NH_3 gas based on the TDLAS detection method, with a minimum detection limit of 0.16×10^{-6} [30]. Additionally, TDLAS gas detection technology has broad application prospects in industrial process safety monitoring [31], gas pipeline leak detection [32], combustion process diagnosis [33], and biomedical detection [34]. However, when used for multi-gas detection, the TDLAS detection technology shows poor accuracy and remarkable detection errors [35, 36]. This phenomenon is mainly costed by the aligning–crossing, and overlapping between absorption lines of the tested gases.

The contents of CO, C_2H_2, and C_2H_4 in coal spontaneous combustion index gases are in the order of 10^{-6} (ppm). Therefore, a long optical path gas absorption cell needs to be used to improve the detection sensitivity. C_2H_2, CH_4, and C_2H_4 are hydrocarbon gases; their molecular structures are similar, the absorption lines have cross-interference, and the trace detection accuracy is low. The near-infrared absorption line of C_2H_4 has some problems, such as poor single peak characteristics and self-spectral line-aliasing interference. Its trace detection sensitivity is low. To solve this problem, this study simulates the spectral distribution of absorption lines for six gases of CSC, including CO, CO_2, CH_4, C_2H_4, C_2H_2, and O_2. Based on the simulation results, optimal absorption lines with restrained aligning–crossing and overlapping are carefully screened. The sensing performance of the detection system based on these optimal absorption lines is evaluated. This study provides an effective basis for accurate monitoring, determining the risk, and actively preventing bituminous coal spontaneous combustion disasters.

Methodology. The Pacific Northwest National Laboratory (PNNL) database, which provides the characteristic parameters of gas absorption lines, is widely used in gas detection [37]. In this study, the absorption lines of index gases of CSC were simulated, including CO, CO_2, CH_4, C_2H_4, C_2H_2, and O_2. The optimal absorption line for each gas was carefully chosen for high sensitivity and accuracy in detection. The screened absorption lines were minimally overlapped with other gases, and the interference between them was restrained. Absorption strength at screened absorption lines was also relatively strong to avoid the influence of background noise, whereas the basement of screened absorption lines was flattened to reduce the line shape aberration.

Screening of absorption lines for multicomponent gases in CSC. Because tunable lasers in the near-infrared spectral range are mature and inexpensive, CO, CO_2, CH_4, and C_2H_2 absorption lines in the 1500- to 1670-nm band were selected. However, O_2 is non-absorbing in the near-infrared band but features strong absorption lines in the visible band, as shown in Fig. 1a. Thus, absorption lines at around 760 nm were screened for O_2. As shown in Fig. 1b, the absorption lines of these gases are well separated. For CO, CO_2, and C_2H_2, most absorption lines are allocated in spectral bands of 1560–1600, 1565–1590, and 1510–1545 nm, respectively. Overall, owing to similar spectral positions and comparable absorption strengths, the cross-aliasing and overlapping between absorption lines of CO and CO_2 are pronounced, making the screening of their absorption lines very complicated. Meanwhile, as absorption lines are well-separated from other gases, it is much easier to choose the optimal absorption line for C_2H_2.

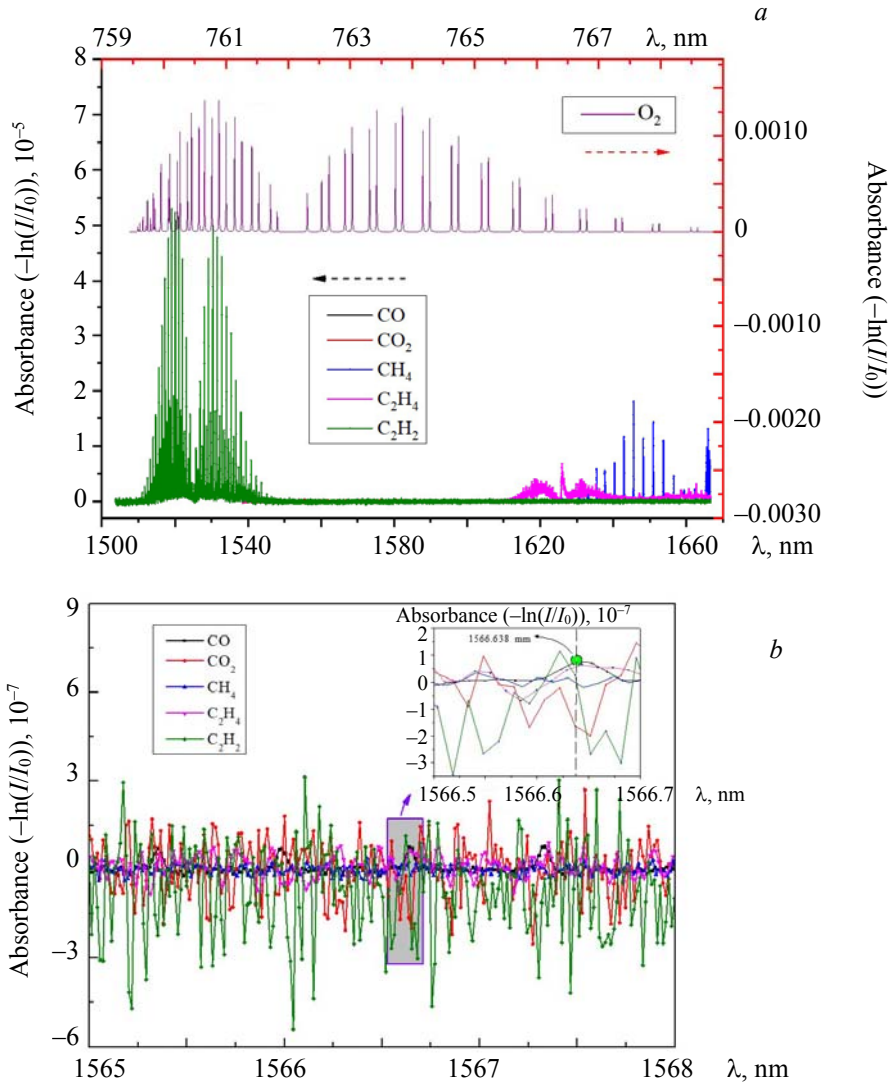

Fig. 1. Distribution of absorption spectrum of multicomponent gas of CSC in (a) 1500–1670 nm and (b) 1565–1568 nm bands.

Compared with other gases, the absorption of CO is much weaker, and its absorption lines strongly overlap those of other gases. The absorption strength of CO near 1566.6 nm is stronger by 2–3 orders of magnitude than that of CO_2, CH_4, and C_2H_2, as shown by the high-resolution absorption spectra in Fig. 2. Thus, the cross-aliasing caused by these gases can be ignored. However, although the absorption strengths of CO and C_2H_4 near 1566.6 nm are comparable, the influence of C_2H_4 is negligible because the concentration of C_2H_4 is much lower than that of CO in the practical application fields. Thus, the wavelength of the tunable laser for CO detection was screened to be 1566.638 nm. Figure 2 shows the absorption line of CO at around 1566.638 nm. As shown in Fig. 3, the absorption strength of CO_2, around 1572.322 nm, is much stronger than that of other gases. Thus, the central wavelength of the CO_2 gas laser was chosen to be 1572.322 nm. As demonstrated in Fig. 4, most of the C_2H_4 gas absorption lines are allocated in the spectrum range of 1625–1627 nm and strongly overlapped with CH_4 gas absorption lines. Based on the principle shown above, 1626.343 nm was chosen as the working wavelength of the tunable laser for C_2H_2 detection.

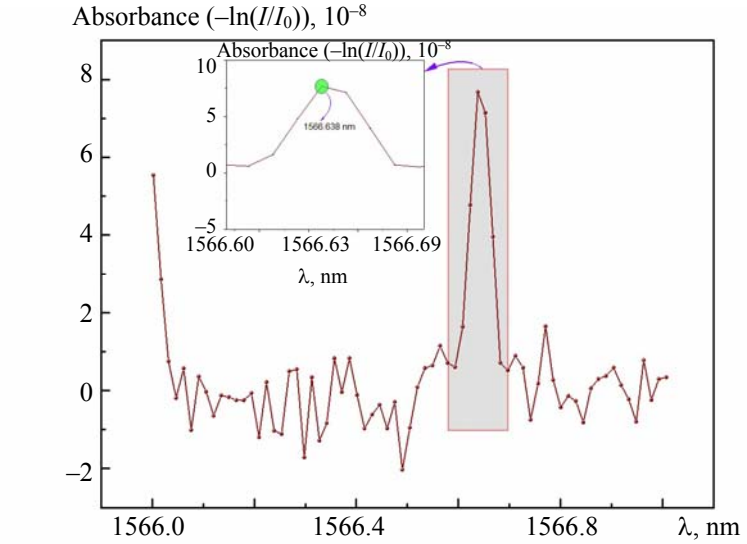

Fig. 2. Distribution of CO gas absorption spectrum at 1566.638 nm central wavelength.

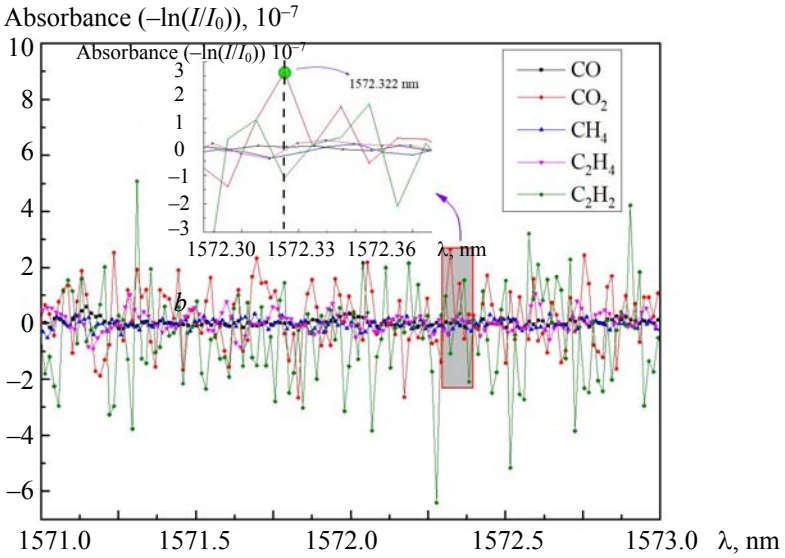

Fig. 3. Distribution of absorption spectrum of multicomponent gas of CSC in 1571–1573 nm band.

Unlike CO, CO_2, and C_2H_4, absorption lines of CH_4, C_2H_2, and O_2 are well separated from their counterparts. Thus, absorption lines were screened based on the absorption strength of these gases as the optimal absorption line is the one with the highest absorption. Consequently, the working wavelengths of the lasers for these gases were chosen to be 1653.721, 1625.945, and 760.654 nm, respectively, as illustrated in Fig. 5–7.

Table 1 presents the wavelength, wavenumber, and the corresponding absorption strength of the chosen absorption line for each gas.

TABLE 1. Optimal Characteristic Absorption Spectrum and Absorbance of CSC Gases

Parameter	CO	CO_2	CH_4	C_2H_4	C_2H_2	O_2
Wavelength, nm	1566.64	1572.32	1653.72	1626.34	1530.37	760.65
Absorption line, cm^{-1}	7.68×10^{-8}	2.65×10^{-7}	1.10×10^{-5}	3.84×10^{-6}	5.00×10^{-5}	1.37×10^{-3}
Absorbance, $cm^{-1}\cdot mol^{-1}\cdot cm^2$	6385.77	6360.02	6046.97	6148.76	6534.36	13146.58

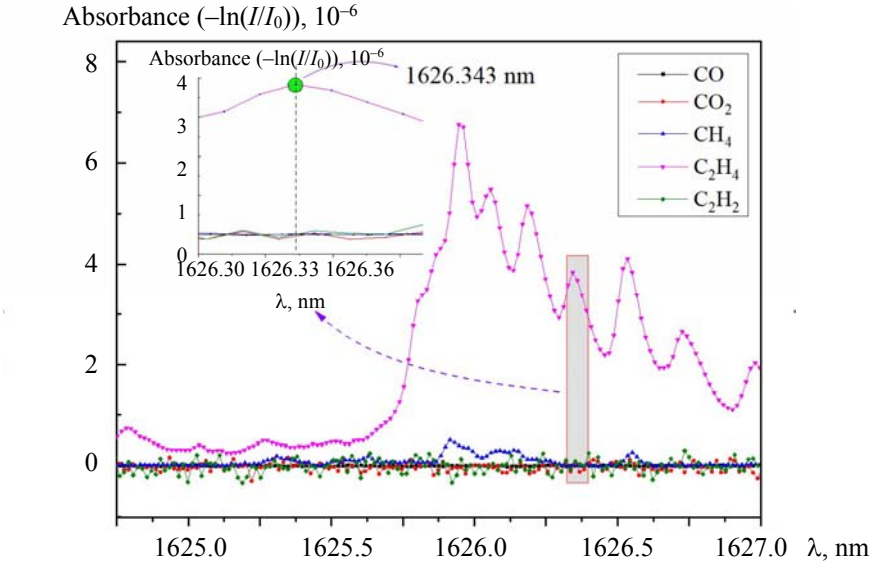

Fig. 4. Distribution of C_2H_4 gas absorption spectrum at 1626.343 nm central wavelength.

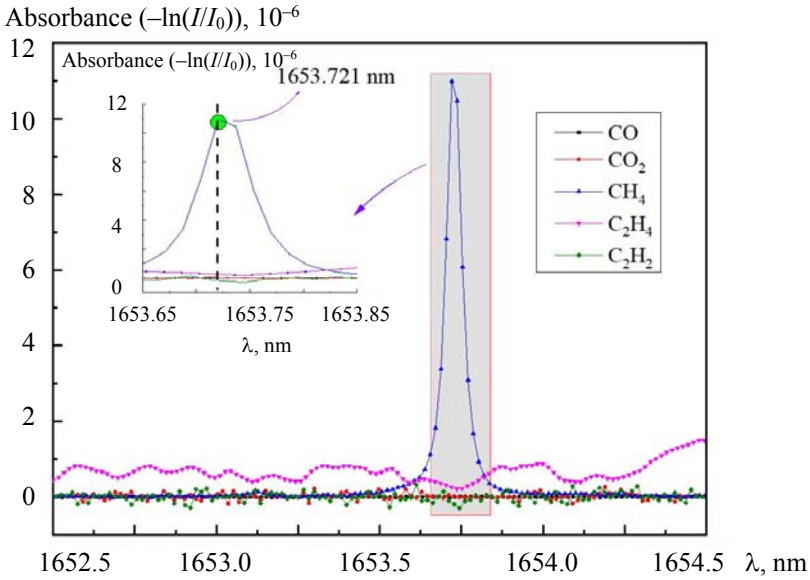

Fig. 5. Distribution of CH_4 gas absorption spectrum at 1653.72 nm central wavelength.

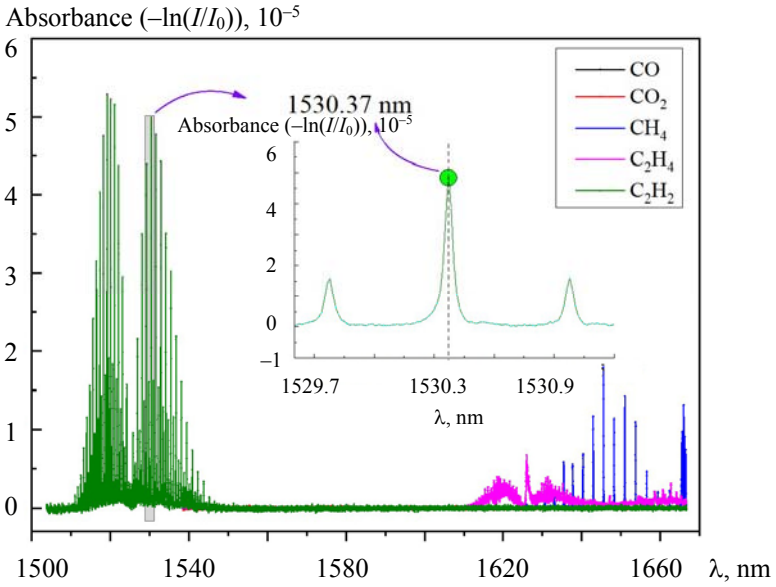

Fig. 6. Distribution of C_2H_2 gas absorption spectrum at 1530.37 nm central wavelength.

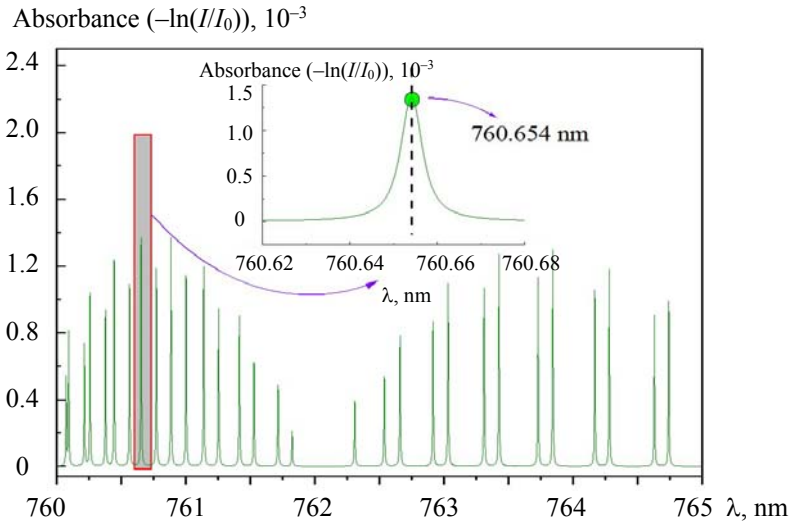

Fig. 7. Distribution of O_2 gas absorption spectrum at 760.65 nm central wavelength.

Performance evaluation of CSC multicomponent gas detection system based on TDLAS. *Experimental system.* Based on the multiplex phase-locked technology, the TDLAS multicomponent gas detection experimental system for spontaneous coal combustion is designed, as shown in Fig. 8. Specifically, this includes DFB lasers with the following six wavelengths: 1566.64 (CO), 1572.32 (CO_2), 1653.72 (CH_4), 1530.37 (C_2H_2), 1626.34 (C_2H_4), and 760.65 nm (O_2). The experimental system comprised a VCSEL laser, fiber splitter, Herriott cell with an optical path of 14.4 m (suitable for gas with near-infrared wavelength), direct optical path absorption cell with an optical path of 30 cm (suitable for oxygen gas), VCSEL laser-driving circuit, DFB laser-driving circuit, photodetector (silicon photodiode, 200–1100 nm, Ø1 mm; FGA10 indium gallium arsenic photodiode, 800–1800 nm, Ø1.0 mm), digital phase-locked amplifier, multi-channel data acquisition card, and a computer. The ambient temperature was 25°C, the gas pressure was 1 atm, the working temperature of the DFB laser was 30°C, the frequency of high-frequency sine wave modulation signal was 5 kHz, the current range of low-frequency sawtooth wave scanning was 20–60 mA, and the scanning frequency was 10 Hz.

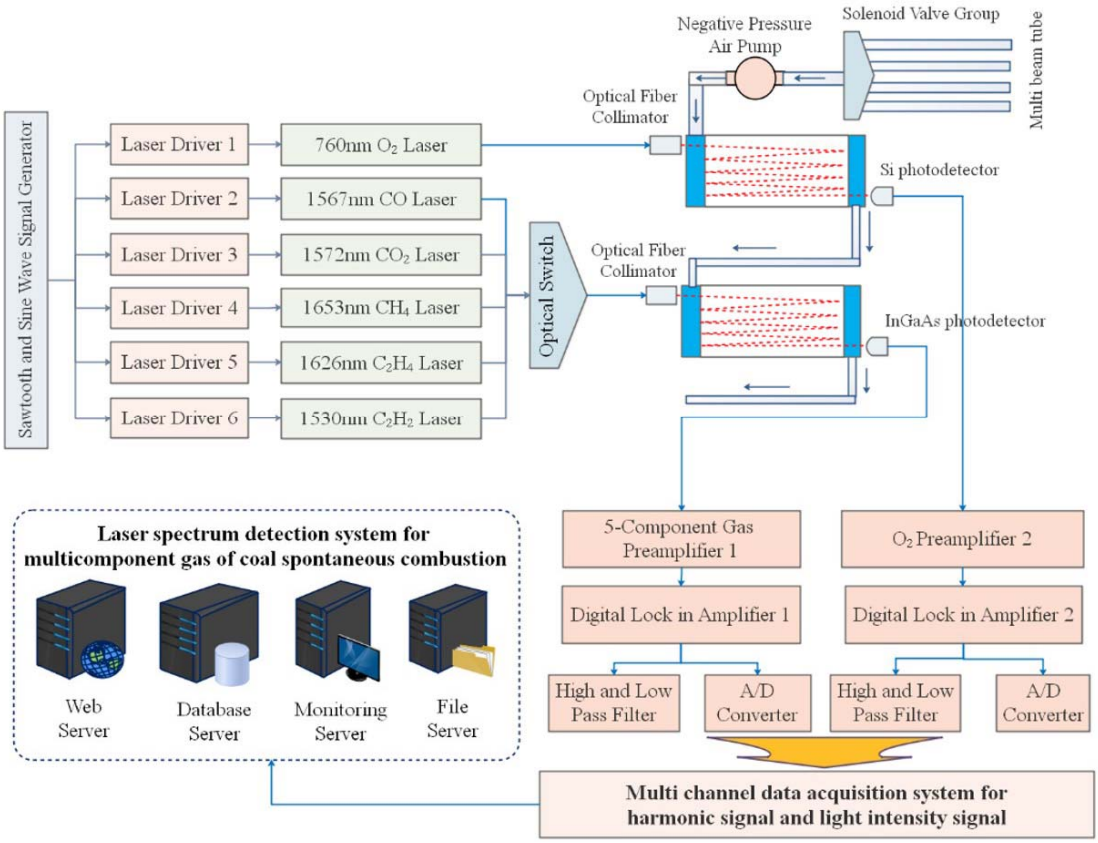

Fig. 8. TDLAS detection experimental system for CSC multicomponent gas.

Detection accuracy. Based on the above-mentioned chosen absorption lines, a detection system was set up to measure multicomponent gases in CSCs. To increase the detection accuracy, the detection system was preheated for 30 min and then pumped for 30 min using standard gas flow at a speed of 400 mL/min. According to the recorded data, as shown in Fig. 9, the average concentrations of tested gases estimated were 49.99×10^{-6}, 200.81×10^{-6}, 106.15×10^{-6}, 106.28×10^{-6}, 50.09×10^{-6}, and 0.52% for CO, CO_2, CH_4, C_2H_4, C_2H_2, and O_2, respectively, and corresponding relative detection errors were 0.62, 0.51, 3.06, 4.20, 0.58, and 1.96%, respectively. Compared with the standard absorption spectrum technologies based on the strongest absorption line, the detection accuracy of the established detection system has been improved by more than 10%.

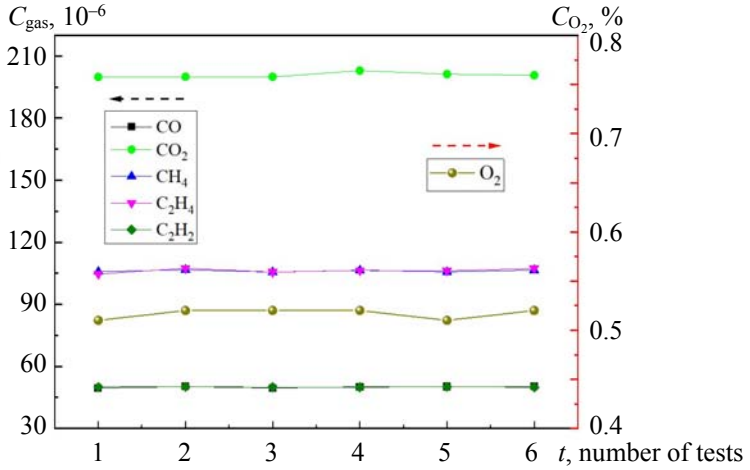

Fig. 9. Test results of accuracy for the TDLAS gas detection system.

Detection limit. Stability is an important index for evaluating the TDLAS gas detection system (Fig. 10). The detection limit can be obtained using the average value of multiple detection data. Allen variance is often used to evaluate and analyze the stability of a TDLAS gas detection system. The minimum value of the Allen variance is the optimal detection time of the system. In this study, the detection result is the lower detection limit of the system, and the optimal detection time represents the system's stability. According to Lan et al. [38], the lower detection limit of the TDLAS gas detection system can be characterized by *Var* (*a*, *m*):

$$Var(A) = \sigma^2, \quad (1)$$

where *a* is the average value of the detection data and σ^2 is the variance.

Mixed calibration gases with different concentrations were measured for 30 min to estimate the detection limit of the detection system. Figure 10 shows the Allan deviations for six tested gases calculated using Eq. (1). Although ensuring that the established system is capable of monitoring the degree of CSC, the detection limits were estimated to be 3.47×10^{-6}, 4.56×10^{-6}, 0.53×10^{-6}, 2.85×10^{-6}, 0.33×10^{-6}, and 1581×10^{-6}, for CO, CO_2, CH_4, C_2H_4, C_2H_4, and O_2, respectively. The corresponding integration times were 27, 20, 52, 56, 35, and 50 s, respectively.

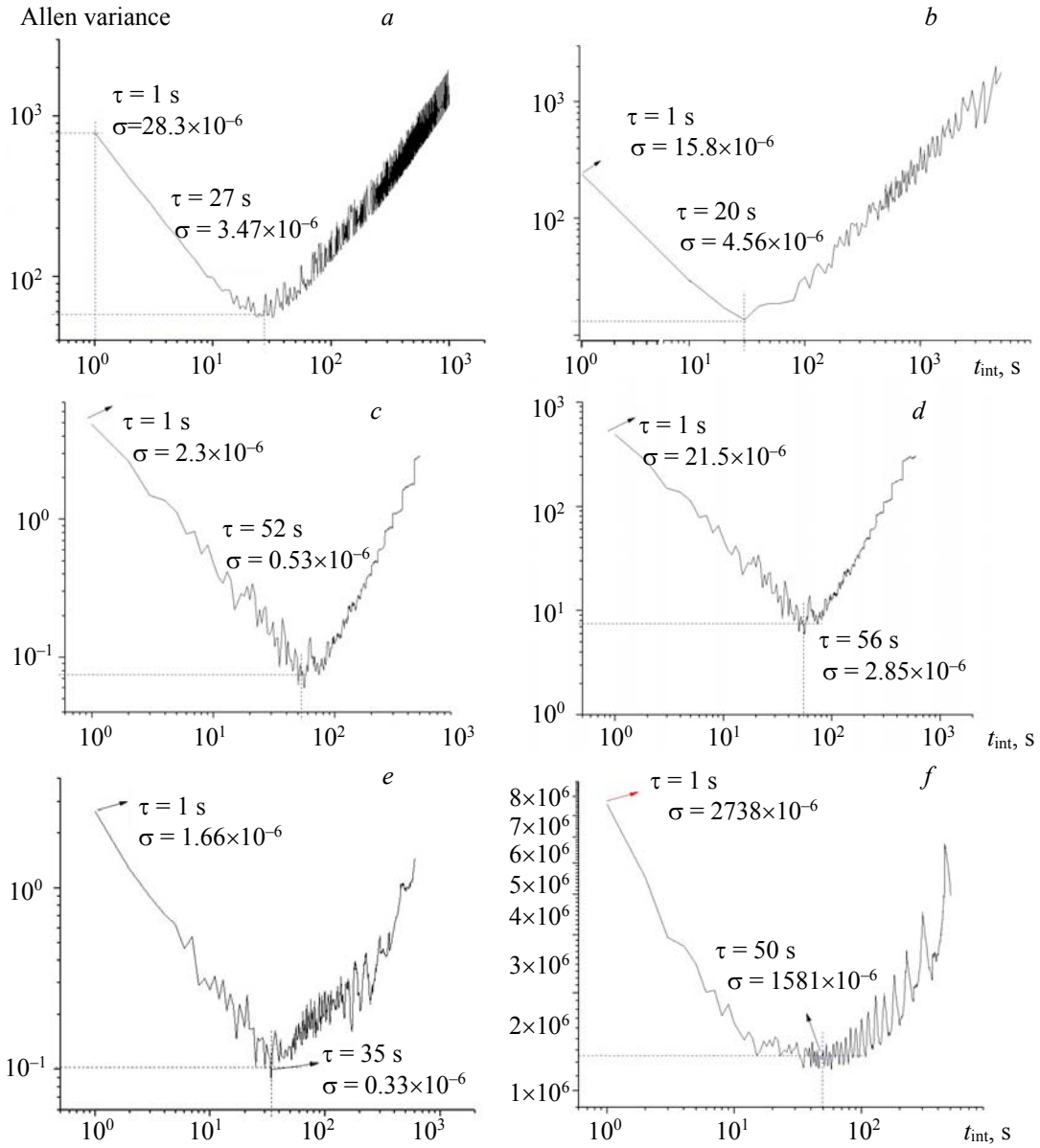

Fig. 10. Evaluation results of Allen variance of detection concentration of multicomponent gas in CSC: (a) Allen variance evaluation result of CO, (b) CO_2, (c) CH_4, (d) C_2H_4, (e) C_2H_2, and (f) O_2.

Conclusions. This study simulated the absorption lines of coal spontaneous combustion multicomponent gases using parameters from the PNNL database. The operation wavelengths of tunable lasers used for gas detection have been carefully screened to overcome the cross-aliasing and overlapping between these absorption lines, which are 1566.64, 1572.32, 1653.72, 1626.34, 1530.37, and 760.65 for CO, CO_2, CH_4, C_2H_4, C_2H_2, and O_2, respectively. A detection system based on these lasers was established for measuring multicomponent gases of coal spontaneous combustion. The experimental results show that the relative errors of the detection system are 0.62, 0.51, 3.06, 4.20, 0.58, and 1.96%, respectively. Based on the Allan variance, the detection limit of the established system is estimated to be 3.47×10^{-6}, 4.56×10^{-6}, 0.53×10^{-6}, 2.85×10^{-6}, 0.33×10^{-6}, and 1581×10^{-6}. The sensing performance of the established detection system satisfies the requirements for the practical application of spontaneous combustion inspection and early warning in bituminous coal mines.

Acknowledgments. This work was supported by the National Key R & D Plan of China (No. 2021YFE0105000), the National Natural Science Foundation of China (No. 52074213), Shaanxi key R & D Plan Project (Nos. 2021SF-472 and 2021GY-131), Yulin Science and Technology Plan Project (Nos. CXY-2020-036 and CXY-2020-037), Science and Technology Fund for outstanding young people of Xi'an University of Science and Technology (No. 2019YQ2-01), Xi'an Science and Technology Plan Project (No. 2020KJRC0068).

REFERENCES

1. Z. Q. Tang, S. Q. Yang, G. Xu, M. Sharifzadeh, *Proc. Saf. Environ.*, **132**, 182–188 (2019).
2. Y. W. Song, S. Q. Yang, X. C. Hu, W. X. Song, N. W. Sang, J. W. Cai, Q. Xu, *Proc. Saf. Environ.*, **129**, 8–16 (2019).
3. W. C. Zheng, S. Q. Yang, W. Z. Li, J. Wang, *Fire Mater.*, **44**, No. 5, 660–672 (2020).
4. B. Du, Y. T. Liang, F. C. Tian, *Fire Safety J.*, **121**, 103298 (2021).
5. W. C. Xia, Y. J. Li, C. K. Niu, *Energ. Source A*, **41**, No. 9, 1110–1115 (2019).
6. H. Q. Zhu, K. Sheng, Y. L. Zhang, S. H. Fang, Y. L. Wu, *PLoS One*, **13**, No. 8, 0202724 (2018).
7. Q. Xu, S. Q. Yang, J. W. Cai, B. Z. Zhou, Y. A. Xin, *Proc. Saf. Environ.*, **118**, 195–202 (2018).
8. L. Ma, R. Z. Guo, M. M. Wu, W. F. Wang, L. F. Ren, G. M. Wei, *Proc. Saf. Environ.*, **142**, 370–379 (2020).
9. T. Ma, X. K. Chen, X. W. Zhai, Y. E. Bai, *RSC Adv.*, **9**, No. 56, 32476–32489 (2019).
10. H. C. Ji, W. Zeng, Y. Q. Li, *Nanoscale*, **11**, No. 47, 22664–22684 (2019).
11. W. Li, W. X. Luo, M. Y. Li, L. Y. Chen, L. Y. Chen, G. Hua, M. J. Yu, *Front. Chem.*, **9**, 723186 (2021).
12. M. M. Kmiec, D. Tse, P. Kuppusamy, *Adv. Exp. Biol.*, **1269**, 259–263 (2021).
13. J. E. Welke, K. C. Hernandes, K. P. Nicolli, J. A. Barbara, A. C. T. Biasoto, C. A. Zini, *J. Sep. Sci.*, **44**, No. 1, 135–168 (2021).
14. H. Sun, Y. B. Shi, X. Ding, X. B. Ding, H. B. Wu, *IEEE Access*, **9**, 51983–51995 (2021).
15. Y. S. H. Parkhangil, *J. Sensor Sci. Technol.*, **27**, No. 5, 294–299 (2018).
16. Z. L. Cui, X. X. Zhang, D. C. Chen, Y. Li, Y. F. Wang, Y. Zhang, H. Wang, *Appl. Spectrosc.*, **75**, No. 3, 265–273 (2021).
17. V. Vitvitsky, R. Banerjee. *Hydrogen Sulfide Redox Biology A*, **554**, 111–123 (2015).
18. Y. C. Lin, F. Liu, X. G. He, W. Jin, M. Zhang, *Opt. Express*, **25**, No. 25, 31568 (2017).
19. C. Lindner, J. Kunz, S. J. Herr, S. Wolf, J. Kiebling, *Opt. Express*, **29**, No. 3, 4035–4047 (2021).
20. R. N. Sa, L. B. Bu, Q. Wang, J. Zhou, *Optik*, **149**, 113–124 (2017).
21. Z. L. Cui, X. X. Zhang, Z. Cheng, Y. L. Li, H. Xiao, *Spectrochim. Acta A*, **215**, 187–195 (2019).
22. M. Reeves, M. Musculus, P. Farrell, *Appl. Optics*, **37**, No. 28, 6627–6635 (1998).
23. C. W. Wen, X. Huang, C. L. Shen, *J. Raman Spectrosc.*, **51**, No. 5, 781–787 (2020).
24. S. L. Zha, H. L. Ma, C. L. Zha, X. Y. Cai, Y. Y. Li, *J. Near Infrared Spec.*, **28**, No. 4, 236–242 (2020).
25. K. L. Mackay, A. Chanda, G. Mackay, J. T. Pisano, T. D. Durbin, K. Crabbe, T. Smith, *J. Appl. Spectrosc*., **83**, No. 4, 627–633 (2016).
26. J. M. Rey, M. Fill, F. Felder, M. W. Sigrist, *Appl. Phys. B-Lasers O*, **117**, No. 3, 935–939 (2014).
27. P. Werle, R. Muckel, F. D'Amato, T. Lancia, *Appl. Phys. B-Lasers O*, **67**, No. 3, 307–315 (1995).
28. U. Gustafsson, J. Sandsten, S. Svanberg, *Appl. Phys. B-Lasers O*, **71**, No. 6, 853–857 (2000).
29. C. Murzyn, A. Sims, H. Krier, N. Glumac, *Opt. Laser. Eng.*, **110**, No. 11, 186–192 (2018).
30. X. Q. Guo, F. Zheng, C. L. Li, X. F. Yang, N. Li, *Opt. Laser. Eng.*, **115**, No. 4, 243–248 (2019).

31. A. Sepman, Y. Ögren, Z. Qu, H. Wiinikka, F. M. Schmidt, *P. Combust. Inst.*, **36**, No. 3, 4541–4548 (2017).
32. H. Xia, W. Q. Liu, Y. J. Zhang, R.F. Kan, Y. B. Cui, M. Wang, Y. He, X. J. Cui, J. Ruan, H. Geng, *Spectrosc. Spectr. Anal.*, **29**, No. 3, 844–847 (2009).
33. R. F. Kan, H. H. Xia, Z. Y. Xu, L. Yao, J. Ruan, *Chin. J. Lasers*, **45**, No. 9, 67–82 (2018).
34. C. Y. Jiang, M. X. Sun, Y. X. Li, C. J. Wang, *Chin. J. Lasers*, **45**, No. 2, 197–205 (2018).
35. M. Jiang, W. B. Feng, H. Gao, M. Zhang, X. N. Meng, *J. Chin. Coal Soc.*, **46**, No. 7, 1–6 (2021).
36. L. Jiang, H. Xia, F. Dong, T. Pang, B. Wu, *Opt. Precis. Eng.*, **21**, No. 11, 2771–2777 (2013).
37. T. J. Johnson, K. D. Hughey, T. A. Blake, W. S. Steven, L. M. Tanya, L. S. Robert, *J. Phys. Chem. A*, **125**, No. 17, 3793–3801 (2021).
38. L. J. Lan, J. Chen, Y. C. Wu, Y. Bai, Y. F. Li, *IEEE T. Instrum. Meas.*, **68**, No. 4, 1140–1147 (2019).